ACS OMEGA

http://pubs.acs.org/journal/acsodf

Article

Design, Synthesis, ADME, and Anticancer Studies of Newer *N*-Aryl-5-(3,4,5-Trifluorophenyl)-1,3,4-Oxadiazol-2-Amines: An Insight into Experimental and Theoretical Investigations

Mohit Agarwal, Obaid Afzal, Salahuddin, Abdulmalik Saleh Alfawaz Altamimi, Mubarak A. Alamri, Manal A. Alossaimi, Vandana Sharma,* and Mohamed Jawed Ahsan*

Cite This: *ACS Omega* 2023, 8, 26837−26849

Read Online

ACCESS | Metrics & More | Article Recommendations | Supporting Information

ABSTRACT: In continuance of our investigation into the anticancer activity of oxadiazoles, we report here the preparation of 10 new 1,3,4-oxadiazole analogues using the scaffold hopping technique. We have prepared the oxadiazoles having a common pharmacophoric structure (oxadiazole linked aryl nucleus) as seen in the reported anticancer agents IMC-038525 (tubulin inhibitor), IMC-094332 (tubulin inhibitor), and FATB (isosteric replacement of the S of thiadiazole with the O of oxadiazole). All of the oxadiazole analogues were predicted for their absorption, distribution, metabolism, and excretion (ADME) profiles and toxicity studies. All of the compounds were found to follow Lipinski's rule of 5 with a safe toxicity profile (Class IV compound) against immunotoxicity, mutagenicity, and toxicity. All of the compounds were synthesized and characterized using spectral data, followed by their anticancer activity tested in a single-dose assay at 10 μM as reported by the National Cancer Institute (NCI US) Protocol against nearly 59 cancer cell lines obtained from nine panels, including non-small-cell lung, ovarian, breast, central nervous system (CNS), colon, leukemia, prostate, and cancer melanoma. *N*-(2,4-Dimethylphenyl)-5-(3,4,5-trifluorophenyl)-1,3,4-oxadiazol-2-amine (**6h**) displayed significant anticancer activity against SNB-19, OVCAR-8, and NCI-H40 with percent growth inhibitions (PGIs) of 86.61, 85.26, and 75.99 and moderate anticancer activity against HOP-92, SNB-75, ACHN, NCI/ADR-RES, 786-O, A549/ATCC, HCT-116, MDA-MB-231, and SF-295 with PGIs of 67.55, 65.46, 59.09, 59.02, 57.88, 56.88, 56.53, 56.4, and 51.88, respectively. The compound **6h** also registered better anticancer activity than Imatinib against CNS, ovarian, renal, breast, prostate, and melanoma cancers with average PGIs of 56.18, 40.41, 36.36, 27.61, 22.61, and 10.33, respectively. Molecular docking against tubulin, one of the appealing cancer targets, demonstrated an efficient binding within the binding site of combretastatin A4. The ligand **6h** (docking score = −8.144 kcal/mol) interacted π-cationically with the residue Lys352 (with the oxadiazole ring). Furthermore, molecular dynamic (MD) simulation studies in complex with the tubulin-combretastatin A4 protein and ligand **6h** were performed to examine the dynamic stability and conformational behavior.

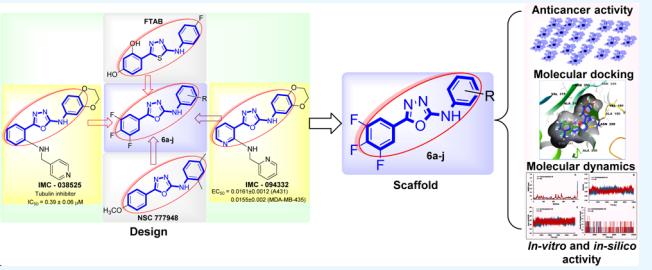

1. INTRODUCTION

Cancer is a group of diseases characterized by the uncontrolled growth and spread of abnormal cells, which can result in death if left untreated. Nearly 10 million cancer deaths and 19.3 million new cases were reported worldwide in 2020. In comparison to 2020, the number of new cases is expected to increase by nearly 1.5 times by 2040. The previous year's statistics in the United States reported nearly 1,918,030 new cancer cases and 609,360 cancer deaths.[1,2] In India, the estimated number of cancer cases in 2022 was 14,61,427, with a 12.8% increase expected by 2025.[3] Despite significant advances in understanding the molecular mechanisms of cancer pathogenesis, there is no single treatment that can completely cure the disease. Various approaches, such as chemotherapy, surgery, radiation therapy, and immunologic treatment, are used to treat cancer depending on its specific type, location, and stage.[4] The use of high doses of radiation to execute cancer cells has advanced significantly in recent years.[5] Immunotherapies are used to treat cancer, but less frequently than chemotherapy, surgery, and radiotherapy. Chemotherapy is a popular cancer treatment that effectively treats a wide range of cancers. However, it frequently has unintended consequences, such as causing damage to healthy cells.[6] As a result, there is an ongoing need for the development of effective anticancer drugs with few side effects. Scientists can create effective anticancer drugs by modifying the chemical

Received: March 4, 2023
Accepted: July 5, 2023
Published: July 20, 2023

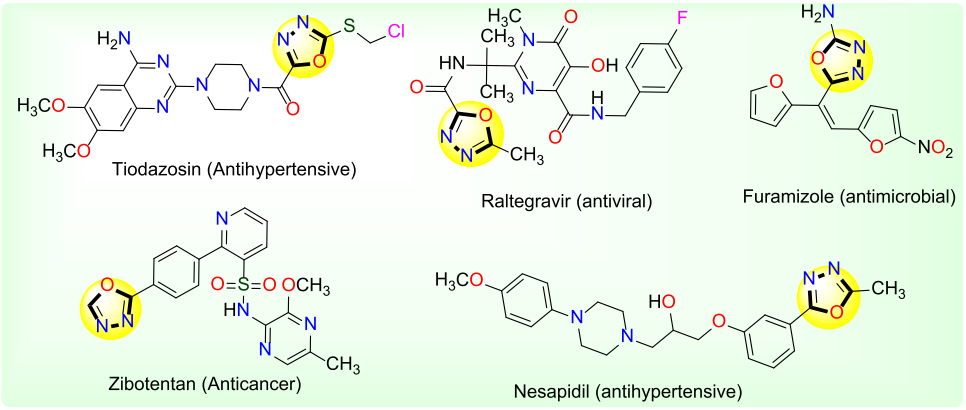

Figure 1. 1,3,4-Oxadiazole-containing agents.

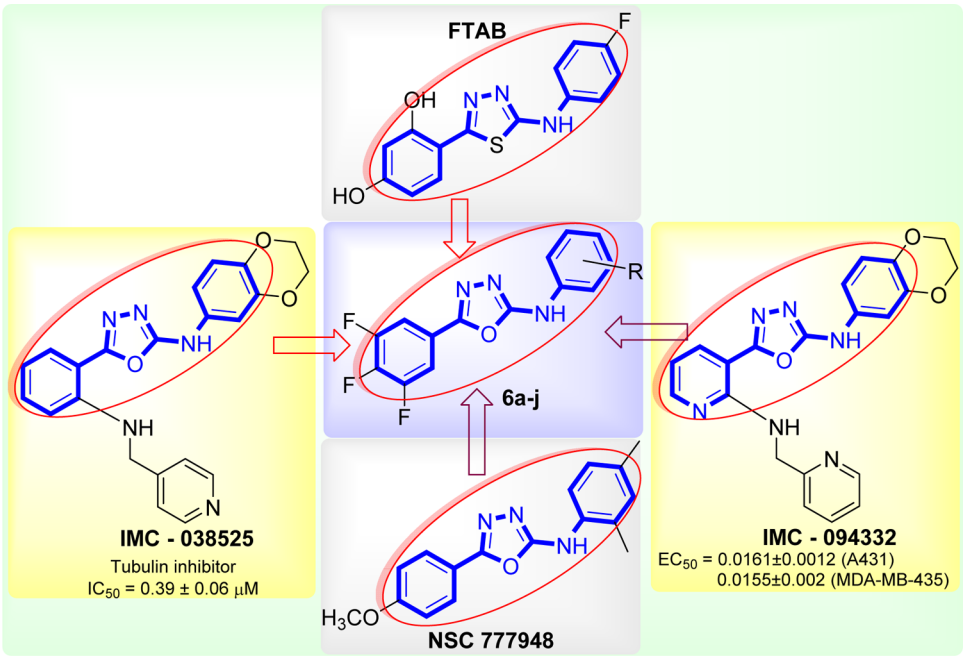

Figure 2. Design of *N*-aryl-5-(3,4,5-trifluorophenyl)-1,3,4-oxadiazol-2-amines (**6a**−**j**) based on the scaffold hopping technique.

structures of bioactive compounds using the structure−activity relationship (SAR) method. A substantial amount of research has been conducted using SAR tools to advance new and compelling anticancer agents.[7,8] Due to long-term treatment and nonspecific drugs, current cancer drug therapies have a small margin of safety and the majority of them result in resistance during therapy. Medicinal chemists are developing newer target-specific anticancer agents in response to the statistical and clinical data gathered.[9−11]

The development of anticancer drugs requires the use of compounds with a variety of heterocyclic molecular structures. Medicinal chemists are working to create novel bioactive drugs based on molecular recognition. Nitrogen-based heterocycles have recently been the focus of extensive research due to their broad spectrum of pharmacological effects.[12−16] Based on where the nitrogen and oxygen atoms are located within the ring, oxadiazoles can be divided into four isomers: 1,2,3-oxadiazole, 1,2,4-oxadiazole, 1,2,5-oxadiazole, and 1,3,4-oxadiazole.[17] The oxadiazole nucleus contains an azole (−N═C−O) moiety, which increases the lipophilicity of the drug.[16b] The drug's lipophilicity promotes transmembrane diffusion, which transports the drug to its intended site. The exceptionally distinct pharmacokinetic properties of 1,3,4-oxadiazole among these isomers have fascinated the attention of scientists.[18] Furthermore, 1,3,4-oxadiazole heterocycles are excellent bio-isosteres of amides and esters, and their participation in hydrogen-bonding interactions with receptors increases their pharmacological activity significantly.[19] The significance of oxadiazoles among these privileged moieties increased as a result of their application in the development of antiproliferative,[20,21] antimicrobial,[22] antituberculosis,[23] anti-inflammatory,[24] antidiabetic,[25] antifungal,[26] antioxidant,[27] antiseizure,[28] anti-Alzheimer,[29] cardiovascular,[30] and antiviral agents,[31] which encouraged us to investigate oxadiazoles. The clinical trial of the oxadiazole-based hybrid compound zibotentan paves the way for the fabrication of a safe and effective anticancer 1,3,4-oxadiazole-based heterocyclic hybrid.[32] An antiretroviral drug Raltegravir, used to treat HIV,[33] Tiodazosin and Nesipidil, both antihypertensive agents,[34] and Furamizole, an antimicrobial agent,[35] all contain the 1,3,4-oxadiazole nucleus as shown in Figure 1.

https://doi.org/10.1021/acsomega.3c01462
ACS Omega 2023, 8, 26837−26849

Scheme 1. Synthesis of *N*-Aryl-5-(3,4,5-trifluorophenyl)-1,3,4-oxadiazol-2-amines (6a−j)

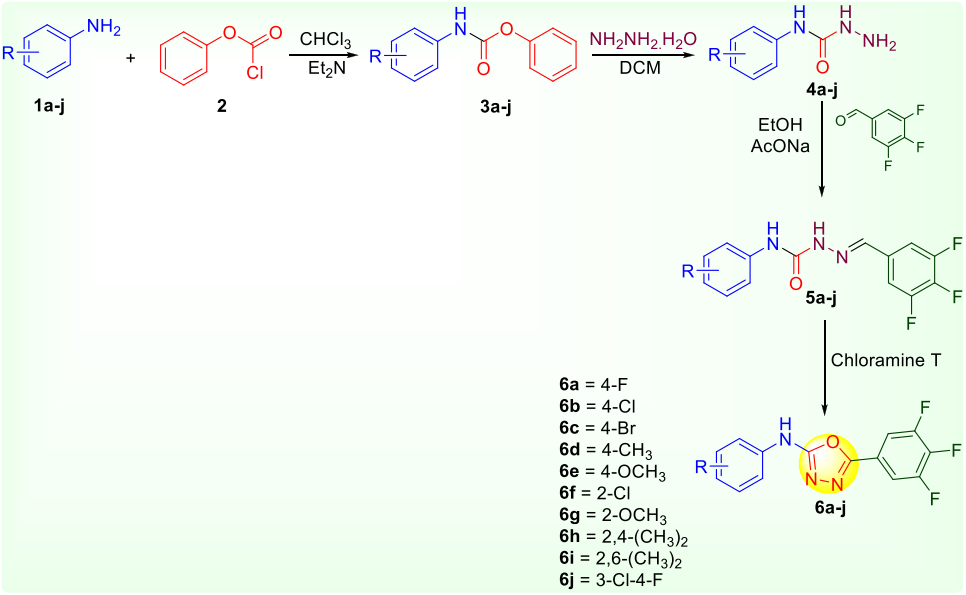

Chromosome separation during cell division, intracellular transport, the growth and maintenance of cell shape, cell motility, and molecule spreading on cell membranes are just a few of the fundamental cellular processes that the microtubule system plays a key role in.[36] Tubulin, the major protein component of microtubules, is what many small molecules are aiming at.[37] As a result, various exertions at preventing mitosis, such as blocking polymerization of tubulin with the tubulin inhibitor, have appeared as an alluring strategy of cancer treatment.[36,38] Breast, lung, ovarian, and other cancers can be successfully treated with microtubule polymerization inhibitors.[39] Several studies have shown that various 1,3,4-oxadiazoles have significant anticancer activity; they significantly inhibited tubulin assembly, slowed down the cell cycle's G2/M phase, and decreased cell growth.[39−42] In the current investigation, we explored and designed a series of 1,3,4-oxadiazole analogues based on scaffold hopping techniques.[43] The pharmacophore of our title compounds was the same as in the IMC-038525, IMC-094332 (phenyl ring replaced by pyridyl ring), NSC 777948, and 1,3,4-thiadiazole derivative (FABT) as shown in Figure 2.[44−46]

2. EXPERIMENTAL SECTION

2.1. General. The synthetic-grade chemicals were procured from Merck, S.D. Fine Chemicals, and Chemco. The melting point and progress of the reaction were analyzed by the open tube capillary method and a preparatory thin-layer chromatography plate (TLC Silica gel 60 F_{254}), respectively. The infrared (IR) spectra were recorded on a Perkin Elmer spectrum. The nuclear magnetic resonance (NMR) spectra were recorded on a Bruker AC 300 MHz spectrometer using tetramethylsilane (TMS) as the internal standard in DMSO-d_6, while the mass spectra were recorded on a Waters ACQUITY TQD.

2.2. General Method of Synthesis of *N*-Aryl-5-(3,4,5-trifluorophenyl)-1,3,4-oxadiazol-2-amines (6a−j). To a solution of (*E*)-*N*-aryl-2-(3,4,5-trifluorobenzylidene)hydrazine-1-carboxamide (**5a−j**) (1 mmol) in absolute ethanol (15 mL), chloramine T (0.625 mmol) was refluxed for 4 h. The TLC spots determined whether the reaction was complete; the reaction solution was finally cooled, and the sodium chloride that had also formed during the reaction was filtered off. Distillation at reduced pressure completely eliminated the surplus ethanol from the filtrate, leaving behind the solid mass, which was then recrystallized with ethanol to obtain *N*-aryl-5-(3,4,5-trifluorophenyl)-1,3,4-oxadiazol-2-amines (**6a−j**).[47]

2.3. ADME and Toxicity Prediction Studies. The ADME prediction studies were carried out online by SwissADME software available online.[48] The toxicity studies were carried out online by ProTox II software.[49]

2.4. In Vitro Anticancer Activity. Using nine diverse panels of 58 or 59 cell lines of cancer, the oxadiazoles (**6a−j**) were evaluated for anticancer activity in a single-dose assay. The anticancer activity was evaluated in accordance with the established National Cancer Institute (NCI US) protocol at a drug concentration of 10 μM.[50−53] The results of anticancer action were designated as growth percent (GP) and percent growth inhibition (PGI). The GP and PGI are correlated as PGI = 100−GP. An in vitro anticancer screening methodology is given in the Supporting Data (available online). NCI US had conducted anticancer compound screening in a one-dose assay.

2.5. Molecular Docking Studies. The ligands **6a−j** were investigated for molecular docking against the tubulin-combretastatin A4 complex. The protein data bank (pdb) provided the X-ray crystallographic structure of the tubulin-combretastatin A4 complex (PDB: 5LYJ) with a resolution of 2.40 Å; *R*-value 0.192 (observed).[54] Chain D was chosen for grid preparation, and the combretastatin A4 binding site was used for ligand docking studies. The ligands **6a−l**, saved as mole files, were used to prepare and minimize ligands for docking by using Ligprep, and the docking was carried out in accordance with the procedure outlined elsewhere.[55]

2.6. Molecular Dynamic Studies. The GROMACS 2018.1 package coupled with OPLS-AA all-atom force fields and the SwissParam server for ligand (**6h** and combretastatin A4) topology parameters was used to run 100 ns MD simulations.[56,57] A study using MD simulation was conducted to verify the mode of interaction and the stability of a potential ligand (**6h**) within the active site of tubulin-combretastatin A4 (PDB ID: 5LYJ). A detailed procedure can be found as Supporting Information available online.

https://doi.org/10.1021/acsomega.3c01462
ACS Omega 2023, 8, 26837−26849

3. RESULTS AND DISCUSSION

3.1. Chemistry. The synthetic protocols that required four steps to prepare the oxadiazole analogues (**6a−j**) are summarized in Scheme 1. In the initial step, a solution of aromatic aniline (**1a−j**) (25 mmol) in trimethyl amine (15 mL) was mixed with a solution of phenyl chloroformate (**2**) (25 mmol; 3.914 g) in chloroform (15 mL) with continuous stirring on a magnetic stirrer for 4−5 h at room temperature to obtain phenyl(substituted phenyl)carbamate (**3a−j**).[58,59] The phenyl(substituted phenyl)carbamate (**3a−j**) (20 mmol) and hydrazine hydrate (40 mmol; 2 mL) in dichloromethane (DCM) were allowed to react at room temperature for 24 h to obtain *N*-[substituted phenyl]hydrazinecarboxamide (**4a−j**).[58,59] In the next step, an equimolar mixture of *N*-[substituted phenyl]hydrazinecarboxamide (**4a−j**) (1.5 mmol) in ethanol was added to a solution of 3,4,5-trifluorobenzaldehyde (1.5 mmol; 240 mg) in ethanol and anhydrous sodium acetate (1.5 mmol) with continuous stirring for 20−30 min at room temperature to form (*E*)-*N*-(substituted phenyl)-2-(3,4,5-trifluorobenzylidene)hydrazine-1-carboxamide (**5a−j**) in good yields.[60] In the final step, (*E*)-*N*-(substituted phenyl)-2-(3,4,5-trifluorobenzylidene)hydrazine-1-carboxamide (**5a−j**) (1 mmol) in 10 mL of absolute ethanol was refluxed by adding chloramine T for 4 h to obtain *N*-aryl-5-(3,4,5-trifluorophenyl)-1,3,4-oxadiazol-2-amine (**6a−j**).[47] The structure of oxadiazoles (**6a−j**) was validated by a spectroscopic technique of infrared (IR), nuclear magnetic resonance (^{1}H and ^{13}C NMR), and mass spectral data. The intermediate compounds (**3a−j** and **4a−j**) had melting points (°C) that were consistent with some of the reported compounds (refer to the Supporting Materials for details).[58−64] All of the synthesized intermediate compounds (**3a−j**, **4a−j**, and **5a−j**) were recrystallized by absolute ethanol, had a sharp melting point, and displayed a single spot on the TLC plates. The intermediate compounds were expected to have an acceptable level of purity as they had a sharp melting point and displayed a single spot on the TLC plate, observed in the iodine or ultraviolet (UV) chamber. The intermediate compounds **5a**, **5e**, **5h**, and **5i** showed a prominent peak at *m*/*z*, 312, 324, 322, and 322 corresponding to their respective molecular mass $(M + 1)^+$. The ^{1}H NMR of the model oxadiazole **6h** showed one singlet at δ ppm 2.20 corresponding to one of the methyl groups (CH_3), while another methyl group (CH_3) was observed as a singlet at δ ppm 2.26; two doublets were observed at δ ppm 6.99 and 7.25 corresponding to the two aromatic protons, while a singlet was observed at δ ppm 7.04 for another aromatic proton of the *N*-phenyl ring; two protons of the halogenated phenyl ring were observed as multiplets at δ ppm 7.84−7.91 and a singlet at δ ppm 8.68 was observed for the secondary amine (ArNH) group. The ^{13}C NMR of the model compound **6h** showed 14 carbon signals at δ ppm 169.37, 164.62, 155.97, 140.16, 139.04, 137.91, 131.73, 128.94, 126.84, 124.96, 116.21, 113.20, 21.73, and 17.90. The ^{1}H and ^{13}C NMR peaks of the representative compound **6h** are shown in Figure 3. The mass spectra of the compound **6h** displayed M^+ and $(M + 1)^+$ peaks at *m*/*z* 319.1 and 320.1, respectively. The characterization data and the national service center (NSC) code of all of the compounds (**6a−j**) are given in Table 1. The color, physical states, percentage yields, and melting point of the intermediate compounds as well as the final compounds are given in the Supporting Information [refer to the Supporting Materials for details].

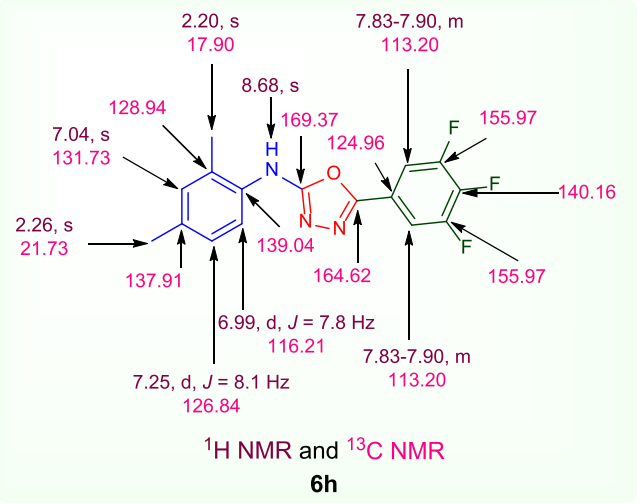

Figure 3. ^{1}H and ^{13}C NMR chemical shift of the representative compound **6h**.

3.2. ADME and Toxicity Prediction. The prediction of ADME was computed from SwissADME software, and their results are given in Table 2.[48] The numbers of rotatable bonds (NROTB ≤10) for the oxadiazole analogues (**6a−j**), the hydrogen-bond acceptor (HBA ≤ 10), and the hydrogen-bond donor (HBD ≤5) were found to be between 3 and 4, between 6 and 7, and 1, respectively. The log *P* (≤5) values were predicted as 2.73−3.23. The molecular weights (M_W ≤ 500) of the oxadiazoles (**6a−j**) were less than 500. The oxadiazole analogues were predicted as orally active substances with good gastrointestinal absorption because none of them violated Lipinski's rule of five.[65] The equation %Abs = 109 ± [0.345 × TPSA] was used to calculate the percent absorption, and the values were found to be between 88.24 and 91.42.[66] Additionally, it was anticipated that six substances would cross the blood−brain barrier (BBB). Apart from ADME prediction, toxicity prediction was also studied for the oxadiazoles (**6a−j**), and their results are given in Table 3. All of the compounds were predicted to be class IV compounds in terms of toxicity and possessed slight hepatotoxicity and carcinogenicity (four compounds), while most of the compounds were predicted as inactive in terms of immunotoxicity, mutagenicity, and cytotoxicity.

3.3. Anticancer Activity. The *N*-aryl-5-(3,4,5-trifluorophenyl)-1,3,4-oxadiazol-2-amines (**6a−j**) were tested for anticancer activity against 58 or 59 NCI cancer cell lines at a single dose of 10 μM drug concentration as per the standard protocol reported elsewhere, and their anticancer data in terms of growth percent (GP) are shown in Table S1 (refer to the Supporting Materials for details) and the percent growth inhibition (PGI) are shown in Table 4. The GP and PGI are correlated as PGI = 100−GP. The cell line UO-31 emerged to be the most sensitive cell line against the tested compounds **6c** and **6e** with PGIs of 20.89 (GP = 79.11) and 13.94 (GP = 86.06), respectively, while K-562 was found to be the most sensitive cell line against the tested compound **6a** with a PGI of 18.47 (GP = 81.53). The cell line NCI-H460 was identified to be the most sensitive cell line against the tested compound **6b** with a PGI of 23.62. The cell lines UACC-62 (PGI = 25.52), MOLT-4 (PGI = 25.26), HCT-116 (PGI = 24.32), and HCT-15 (PGI = 20.46) were found to be the most sensitive cell lines against the tested compound **6g**, while

https://doi.org/10.1021/acsomega.3c01462
ACS Omega 2023, 8, 26837−26849

Table 1. NSC Code and Characterization Data of Oxadiazole Analogues (6a−j)

s. no.	compounds	NSC code	IR (cm^{-1})	^{1}H NMR (300 MHz DMSO-d_6; δ ppm)	^{13}C NMR (75 MHz DMSO-d_6)	elemental analysis and mass
1	**6a**	833186	3212 (NH), 1551 (N═C), 1226 (−O−), 1017 (C−F)	7.08−7.18 (m, 2H, ArH), 7.60−7.67 (m, 2H, ArH), 7.86−7.97 (m, 2H, ArH), 9.06 (s, 1H, ArNH)	169.36, 164.69, 157.39, 151.59, 140.22, 134.57, 124.57, 120.65, 116.35, 113.12	anal. calc. for $C_{14}H_7F_4N_3O$: C, 54.38; H, 2.28; N, 13.59; found: C, 54.18; H, 2.27; N, 13.56%. ESI-MS m/z = 309.1 $(M)^+$, 310.1 $(M + 1)^+$
2	**6b**	833187	3222 (NH), 1595 (N═C), 1317 (−O−), 1016 (C−F), 708 (C−Cl)	7.35 (d, 2H, J = 9.0 Hz, ArH), 7.69 (d, 2H, J = 9.0 Hz, ArH), 7.87−7.97 (m, 2H, ArH), 9.11 (s, 1H, ArNH)	169.37, 164.23, 151.53, 140.31, 137.15, 129.82, 127.74, 125.24, 122.70, 113.14	anal. calc. for $C_{14}H_7ClF_3N_3O$: C, 51.63; H, 2.17; N, 12.90; found: C, 51.59; H, 2.16; N, 12.93%. ESI-MS m/z = 325.1 $(M)^+$, 327.1 $(M + 2)^+$.
3	**6c**	833195	3192 (NH), 1598 (N═C), 1342 (−O−), 1047 (C−F), 694 (C−Br)	7.36−7.51 (m, 2H, ArH), 7.65 (d, 2H, J = 6.0 Hz, ArH), 7.94 (d, 2H, J = 6.0 Hz, ArH), 8.65 (s, 1H, ArNH)	169.37, 164.23, 151.61, 140.24, 137.15, 132.33, 124.95, 118.56, 116.56, 113.14	anal. calc. for $C_{14}H_7BrF_3N_3O$: C, 45.43; H, 1.91; N, 11.35; found: C, 45.40; H, 1.93; N, 11.37%. ESI-MS m/z = 368.9 $(M)^+$, 370.9 $(M + 2)^+$
4	**6d**	833188	3021 (NH), 1595 (N═C), 1140 (−O−), 1044 (C−F)	2.21 (s, 3H, CH_3), 7.03 (d, 2H, J = 8.4 Hz, ArH), 7.27 (d, 2H, J = 8.4 Hz, ArH), 7.85−7.95 (m, 2H, ArH), 8.94 (s, 1H, ArNH)	169.37, 164.56, 151.61, 140.85, 135.88, 131.27, 129.55, 124.59, 120.43, 113.14, 21.32	anal. calc. for $C_{15}H_{10}F_3N_3O$: C, 59.02; H, 3.30; N, 13.77; found: C, 59.05; H, 3.32; N, 13.35%. ESI-MS m/z = 305.1 $(M)^+$, 306.1 $(M + 1)^+$
5	**6e**	833189	3023 (NH), 1597 (N═C), 1181 (−O−), 1044 (C−F)	3.81 (s, 3H, OCH_3), 6.85 (d, 2H, J = 9.0 Hz, ArH), 7.52 (d, 2H, J = 9.0 Hz, ArH), 7.84−7.96 (m, 2H, ArH), 8.92 (s, 1H, ArNH)	169.36, 164.55, 153.26, 151.61, 140.45, 131.87, 124.96, 121.80, 115.15, 113.13, 56.47	anal. calc. for $C_{15}H_{10}F_3N_3O_2$: C, 56.08; H, 3.14; N, 13.08; found: C, 56.05; H, 3.12; N, 13.10%. ESI-MS m/z = 321.1 $(M)^+$, 322.1 $(M + 1)^+$
6	**6f**	833190	3202 (NH), 1584 (N═C), 1314 (−O−), 1044 (C−F), 746 (C−Cl)	7.83−7.92 (m, 2H, ArH), 7.92−8.12 (m, 4H, ArH), 8.95 (s, 1H, ArNH)	169.35, 164.53, 151.74, 140.42, 136.45, 131.96, 127.64, 125.54, 124.96, 122.84, 122.22, 113.87	anal. calc. for $C_{14}H_7ClF_3N_3O$: C, 51.63; H, 2.17; N, 12.90; found: C, 51.60; H, 2.16; N, 12.89%. ESI-MS m/z = 326.1 $(M + 1)^+$, 328.1 $(M + 3)^+$
7	**6g**	833191	3201 (NH), 1589 (N═C), 1343 (−O−), 1045 (C−F)	3.83 (s, 3H, OCH_3), 7.12 (d, 2H, J = 9.0 Hz, ArH), 7.52 (d, 2H, J = 9.0 Hz, ArH), 7.84−7.96 (m, 2H, ArH), 8.91 (s, 1H, ArNH)	169.37, 164.55, 151.61, 147.53, 140.09, 132.70, 124.96, 122.61, 121.80, 113.51, 113.20, 112.09, 56.14	anal. calc. for $C_{15}H_{10}F_3N_3O_2$: C, 56.08; H, 3.14; N, 13.08; found: C, 56.04; H, 3.12; N, 13.06%. ESI-MS m/z = 321.1 $(M)^+$, 322.1 $(M + 1)^+$
8	**6h**	833194	3088 (NH), 1547 (N═C), 1331 (−O−), 1047 (C−F)	2.20 (s, 3H, CH_3), 2.26 (s, 3H, CH_3), 6.99 (d, 1H, J = 7.8 Hz, ArH), 7.04 (1H, s, ArH), 7.25 (d, 1H, J = 8.1 Hz, ArH), 7.83−7.90 (2H, m, ArH), 8.68 (1H, s, ArNH)	169.37, 164.62, 155.97, 140.16, 139.04, 137.91, 131.73, 128.94, 126.84, 124.96, 116.21, 113.20, 21.73, 17.90	anal. calc. for $C_{16}H_{12}F_3N_3O$: C, 60.19; H, 3.79; N, 13.16; found: C, 60.16; H, 3.77; N, 13.13%. ESI-MS m/z = 319.1 $(M)^+$, 320.1 $(M + 1)^+$
9	**6i**	833192	3112 (NH), 1529 (N═C), 1371 (−O	2.25 (s, 6H, CH_3), 7.01−7.09 (m, 3H, ArH), 7.83−7.95 (m, 4H, ArH), 8.74 (s, 1H, ArNH)	169.37, 164.24, 151.68, 140.23, 137.07, 136.07, 128.34, 124.96, 121.25, 113.21, 17.89	anal. calc. for $C_{16}H_{12}F_3N_3O$: C, 60.19; H, 3.79; N, 13.16; found: C, 60.15; H, 3.76; N,

https://doi.org/10.1021/acsomega.3c01462
ACS Omega 2023, 8, 26837−26849

Table 1. continued

s. no.	compounds	NSC code	IR (cm^{-1})	^{1}H NMR (300 MHz DMSO-d_6, δ ppm)	^{13}C NMR (75 MHz DMSO-d_6)	elemental analysis and mass
			−), 1047 (C−F)			13.12%. ESI-MS m/z = 319.1 $(M)^+$, 320.1 $(M + 1)^+$
10	**6j**	833193	3102 (NH), 1529 (N=C), 1371 (−O −), 1047 (C−F), 708 (C−Cl)	7.37 (s, 1H, ArH), 7.62−7.67 (m, 2H, ArH), 7.88−7.69 (m, 2H, ArNH), 9.16 (s, 1H, ArNH)	169.38, 164.55, 151.61, 148.82, 140.16, 139.40, 124.98, 121.56, 118.70, 118.33, 114.26, 113.21	anal. calc. for $C_{14}H_6ClF_4N_3O$: C, 48.93; H, 1.76; N, 12.23; found: C, 48.90; H, 1.78; N, 12.25%. ESI-MS m/z = 343.1 $(M)^+$, 345.1 $(M + 1)^+$

MCF7 (PGI = 23.11) and UO-31 (PGI = 22.03) were revealed to be the most sensitive cell lines against the tested compound **6j**. The compound **6f** demonstrated moderate anticancer activity against the cell lines HCT-116 and MCF7 with PGIs of 67.16 and 57.14, respectively, and less anticancer activity against the cell lines HCT-15, CAKI-1, MOLT-4, K-562, RPMI-8226, COLO 205, NCI-H522, UO-31, MDA-MB-468, UACC-62, CCRF-CEM, HT29, and PC-3 with PGIs of 43.79, 36.5, 32.94, 32.31, 28.92, 26.41, 25.68, 25.32, 24.38, 22.87, 22.46, 22, and 20.46 respectively. The compound **6f** displayed insignificant anticancer activity (PGI <20) against the rest of the 45 cell lines. The compound **6i** demonstrated good anticancer activity against the cell lines MCF7 and HCT-116 with PGIs of 85.39 and 71.08, respectively, moderate anticancer activity against the cell line K-562 with a PGI of 51.8, and less anticancer activity against HT29, HCT-15, PC-3, UO-31, IGROV1, COLO 205, T-47D, RPMI-8226, MOLT-4, NCI-H23, MALME-3M, and CCRF-CEM with PGIs of 41.01, 38.76, 37.29, 31.3, 30.87, 30.81, 28.84, 26.8, 26.23, 24.23, 22.98, and 20.24 respectively. The compound **6i** displayed insignificant anticancer activity (PGI < 20) against the rest of the 43 cell lines. The compound **6d** displayed good anticancer activity against MCF7 with a PGI of 81.94, moderate anticancer activity against HCT-116 with a PGI of 64.47, and less anticancer activity against K-562, HT29, IGROV1, UO-31, COLO 205, PC-3, T-47D, HCT-15, and MALME-3M with PGIs of 47.25, 47.22, 46.1, 31.48, 28.33, 27.62, 27.43, 26.97, and 20.75, respectively. The compound **6d** displayed insignificant anticancer activity (PGI < 20) against the rest of the 47 cell lines. The most promising anticancer activity was shown by the compound **6h**, and it displayed good anticancer activity against SNB-19, OVCAR-8, and NCI-H40 with PGIs of 86.61, 85.26, and 75.99, respectively, moderate anticancer activity against HOP-62, SNB-75, ACHN, NCI/ADR-RES, 786-O, A549/ATCC, HCT-116, and MDA-MB-231 with PGIs of 67.55, 65.46, 59.09, 59.02, 57.88, 56.88, 56.53, 56.4, and 51.88 respectively, and less anticancer activity against U251, NCI-H226, HS 578T, OVCAR-4, SF-268, NCI-H322M, RXF 393, CAKI-1, SK-OV-3, UO-31, SF-539, NCI-H522, SN12C, NCI-H23, PC-3, HOP-92, DU-145, IGROV1, EKXVA, OVCAR-3, and SK-MEL-28 with PGIs of 49.65, 49.55, 48.22, 48.19, 48.16, 45.92, 44.96, 41.91, 41.46, 40.82, 35.31, 30.22, 28.43, 25.81, 23.09, 22.86, 22.13, 21.44, 21.2, 21.18, and 21.05, respectively. The compound **6h** displayed insignificant anticancer activity (PGI < 20) against the rest of the 15 cell lines. The compounds that showed growth inhibitions of ≥68% were considered to be active toward the particular cell lines.[67] The comparative anticancer activities of the synthesized oxadiazole analogues in terms of the PGI scale are given in Table 4. The compounds **6a** and **6e** were found to have insignificant anticancer activity against all of the tested 58 NCI cell lines, while compounds **6d** (MCF7), **6h** (SNB-19, OVCAR-8, and NCI-H40), and **6i** (MCF7 and HCT-116) demonstrated good anticancer activity against a few cancer cell lines. The compound **6d** registered moderate anticancer activity against HCT-116, while the compound **6i** registered moderate anticancer activity against K-562. The compound **6f** registered moderate anticancer activity against HCT-116 and MCF7. The most active compound **6h** demonstrated good anticancer activity against three cancer cell lines including SNB-19 (CNS cancer), OVCAR-8 (ovarian cancer), and NCI-H460 (non-small cell lung cancer). The compound **6h** registered moderate anticancer activity against nine cancer

https://doi.org/10.1021/acsomega.3c01462
ACS Omega 2023, 8, 26837−26849

Table 2. ADME Prediction of Oxadiazole Analogues (6a−j)

s. no.	compound	% ABS	volume	TPSA	NROTB	HBA	HBD	Log *P* (iLOGP)	M_W	BBB permeation	GI absorption	Lipinski's violations
1	**6a**	91.42	232.24	50.95	3	7	1	2.73	309.22	yes	high	0
2	**6b**	91.42	240.85	50.95	3	6	1	2.90	325.67	no	high	0
3	**6c**	91.42	245.20	50.95	3	6	1	2.99	370.12	no	high	0
4	**6d**	91.42	243.87	50.95	3	6	1	2.88	305.25	yes	high	0
5	**6e**	88.24	252.86	60.18	4	7	1	2.93	321.25	yes	high	0
6	**6f**	91.42	240.85	50.95	3	6	1	3.01	325.67	no	high	0
7	**6g**	88.24	252.86	60.18	4	7	1	3.11	321.25	yes	high	0
8	**6h**	91.42	260.43	50.95	3	6	1	3.23	319.28	yes	high	0
9	**6i**	91.42	260.43	50.95	3	6	1	3.23	319.28	yes	high	0
10	**6j**	91.42	245.78	50.95	3	7	1	2.85	343.66	no	high	0

Table 3. Prediction of Toxicities of Oxadiazole Analogues (6a−j)

s. no.	compound	hepatotoxicity	carcinogenicity	immunotoxicity	mutagenicity	cytotoxicity	LD_{50} (mg/Kg)	class
1	**6a**	+	+	−	−	−	550	IV
2	**6b**	+	−	−	−	−	550	IV
3	**6c**	+	+	−	−	−	550	IV
4	**6d**	+	+	−	−	−	550	IV
5	**6e**	+	−	−	−	−	550	IV
6	**6f**	+	−	−	−	−	550	IV
7	**6g**	+	−	−	−	−	1087	IV
8	**6h**	+	+	−	−	−	550	IV
9	**6i**	+	+	−	−	−	550	IV
10	**6j**	+	−	−	−	−	550	IV

cell lines including HOP-62 and A549/ATCC (non-small-cell lung cancer), SNB-75 and SF-295 (CNS cancer), ACHN and 786-0 (renal cancer), NCI/ADR-RES (ovarian cancer), HCT-116 (colon cancer), and MDA-MB-231 (breast cancer). Furthermore, the average PGIs of individual panels were evaluated for each compound (**6a−j**), and comparisons with the standard drug Imatinib are given in Table 5. The oxadiazole analogue **6i** registered maximum anticancer activity against leukemia and colon cancer cell lines with average PGIs of 24.87 and 25.83, respectively, while the oxadiazole analogue **6h** registered better anticancer activity than Imatinib against CNS, non-small-cell lung, ovarian, renal, breast, prostate, and melanoma cancer cell lines with average PGIs of 56.18, 43.99, 40.41, 36.36, 27.61, 22.61, and 10.33, respectively. The anticancer data of Imatinib in the one-dose assay was retrieved with NSC code 759854 from the official website of the National Cancer Institute.[53b] The structure−activity relationship (SAR) established from the mean GP of anticancer data demonstrated that 2,4-dimethyl (**6h**) substitution in the *N*-phenyl ring was found to be the most promising, followed by 2,6-dimethyl (**6i**), 2-chloro (**6f**), and 2-methoxy (**6g**). The electronegative (4-fluoro, 4-chloro, and 4-bromo) substitution at the *para* position and the 3-chloro-4-fluoro substitution were found to be insignificant, while electron-releasing group substitutions (2,4-dimethyl, 2,6-dimethyl, 2-methyl) and electronegative substitution (chloro) at the *ortho* position were found to be significant than at the *para* position. The methoxy substitutions at the *ortho* position were found to be good in comparison to that at the *para* position.

3.4. Molecular Docking Studies. Tubulin is an appealing target for a number of clinical agents, including paclitaxel and the vinca alkaloids vinblastine and vincristine.[68] Several studies have shown that 1,3,4-oxadiazoles have anticancer activity; they inhibited tubulin assembly, reduced cell growth, and caused cells to become stuck in the phase G2/M of the cell cycle.[39−42] We conducted molecular docking experiments with tubulin-combretastatin A4 (PDB ID: 5LYJ), and their results are shown in Table 6. The ligands **6b−e** and **6j** demonstrated efficient binding within the binding site of combretastatin A4, with docking scores ranging from −7.803 to −8.519 kcal/mol with no significant interaction with any residues. The ligands **6a** (docking score = −8.333 kcal/mol), **6f** (docking score = −8.557 kcal/mol), and **6i** (docking score = −8. 839 kcal/mol) demonstrated similar types of interactions within the binding site of tubulin-combretastatin A4 with a H-bond with the amino acid residue Ans258 (with one of the nitrogens of oxadiazole) as shown in Figure S2 (refer to the Supporting Materials for details). The ligand **6g** (docking score = −8. 558 kcal/mol) demonstrated two types of interactions within the binding site of tubulin-combretastatin A4: a H-bond with the residue Ans258 (with one of the nitrogens of oxadiazole) and a π−cationic interaction with the residue Lys352 (with the oxadiazole ring), and accommodated within the hydrophobic pocket containing the residues Cys241, Leu242, Leu255, Met259, Val351, Ala354, and Ile378 as shown in Figure 4. The ligand **6h** (docking score = −8.144 kcal/mol) demonstrated π-cationic interaction with the residue Lys352 (with the oxadiazole ring), and its 2,4-dimethylphenyl ring lies in the hydrophobic pocket containing the residues Ala250, Leu248, Ile378, Ala316, Lue242, Cys241, and Val238, while the 3,4,5-triflurophenyl ring lies within the hydrophobic pocket containing the residues Met259, Ala180, and Val181 as shown in Figure 5. The reference ligand combretastatin A4 did not exhibit significant interaction within the active site of the D-chain; however, it was accommodated within the hydrophobic pocket containing the residues Val238, Cys241, Leu242, leu248, Ala250, Leu255, Met259, Val351, and Ala354. It was found that combretastatin A4 within the active site of the B-chain exhibited a H-bond interaction with the reside Thr179 (of A-chain) as reported in the literature.[55] The π−

https://doi.org/10.1021/acsomega.3c01462
ACS Omega 2023, 8, 26837−26849

Table 4. Comparative Anticancer Activity of Oxadiazole Analogues (6a−j) on the Percent of Growth Inhibitions (% GIs) Scale[a]

	cell line (percent of growth inhibition; % GI)		
compounds	>68	67.99 to 50.00	49.99 to 20.00
6a	-	-	-
6b	-	-	NCI-H460 (23.62)
6c	-	-	UO-31 (20.89)
6d	MCF7 (81.94)	HCT-116 (64.47)	K-562 (47.25)
			HT29 (47.22)
			IGROV1 (46.1)
			UO-31 (31.48)
			COLO 205 (28.33)
			PC-3 (27.62)
			T-47D (27.43)
			HCT-15 (26.97)
			MALME-3M (20.75)
6e	-	-	-
6f	-	HCT-116 (67.16)	HCT-15 (43.79)
		MCF7 (57.14)	CAKI-1 (36.5)
			MOLT-4 (32.94)
			K-562 (32.31)
			RPMI-8226 (28.92)
			COLO 205 (26.41)
			NCI-H522 (25.68)
			UO-31 (25.32)
			MDA-MB-468 (24.38)
			UACC-62 (22.87)
			CCRF-CEM (22.46)
			HT29 (22)
			PC-3 (20.76)
6g	-	-	UACC-62 (25.52)
			MOLT-4 (25.26)
			HCT-116 (24.32)
			HCT-15 (20.46)
6h	SNB-19 (86.61)	HOP-62 (67.55)	U251 (49.65)
	OVCAR-8 (85.26)	SNB-75 (65.46)	NCI-H226 (49.55)
	NCI-H460 (75.99)	ACHN (59.09)	HS 578T (48.22)
		NCI/ADR-RES (59.02)	OVCAR-4 (48.19)
		786-O (57.88)	SF-268 (48.16)
		A549/ATCC (56.88)	NCI-H322M (45.92)
		HCT-116 (56.53)	RXF 393 (44.96)
		MDA-MB-231 (56.4)	CAKI-1 (41.91)
		SF-295 (51.88)	SK-OV-3 (41.46)
			UO-31 (40.82)
			SF-539 (35.31)
			NCI-H522 (30.22)
			SN12C (28.43)
			NCI-H23 (25.81)
			PC-3 (23.09)
			HOP-92 (22.86)
			DU-145 (22.13)
			IGROV1 (21.44)
			EKXVA (21.2)
			OVCAR-3 (21.18)
			SK-MEL-28 (21.05)
6i	MCF7 (85.39)	K-562 (51.8)	HT29 (41.01)
	HCT-116 (71.08)		HCT-15 (38.76)
			PC-3 (37.29)
			UO-31 (31.3)
			IGROV1 (30.87)
			COLO 205 (30.81)
			T-47D (28.84)
			RPMI-8226 (26.8)
			MOLT-4 (26.23)
			NCI-H23 (24.23)
			MALME-3M (22.98)
			CCRF-CEM (20.24)
6j	-	-	MCF7 (23.11)
			UO-31 (22.03)

[a](-) None of the cell lines displayed a growth inhibition of this percentage.

Table 5. Comparative Anticancer Activity of Oxadiazole Analogues (6a−j) and Imatinib on the Percent of Growth Inhibition (% GI) Scale

panels	6a	6b	6c	6d	6e	6f	6g	6h	6i	6j	Imatinib[a]
leukemia	7.26	3.11	−0.72	18.75	−0.28	23.37	13.07	4.26	**24.87**	1.96	9
non-small-cell lung cancer	−3.59	0.32	−2.47	4.37	-4.23	5.711	0.17	**43.99**	7.65	−2.75	15.68
colon cancer	−2.22	−7.14	−5.1	21.16	−13.1	21.20	4.54	15.52	**25.83**	−11.3	5.34
CNS cancer	−3.2	−7.75	0.918	−7.01	−9.31	−5.28	2.57	**56.18**	3.22	−4.3	5.8
melanoma	−2.42	−6.62	−5.11	3.36	−6.36	1.28	1.25	**10.33**	4.31	−6.72	−0.87
ovarian cancer	−6.52	−12.65	−0.06	−1.58	−10.58	2.82	−1.53	**40.61**	3.19	−8.03	−7.16
renal cancer	−4.93	−9.24	−4.8	−4.73	−12.26	0.67	0.89	**36.36**	1.14	−9.87	3.25
prostate cancer	−3.27	−4.74	−9.61	12.16	−16.3	2.86	6.15	**22.61**	17.18	−2.92	12.5
breast cancer	−4.52	−4.28	8.568	17.48	−4.31	13.36	0.69	**27.61**	21.09	−1.62	12.15

[a]Imatinib data were obtained from the NCI website using the NSC code 759854.[53b] The tested compound had the highest anticancer activity on the respective cancer panel, as indicated by the use of a bold font. The PGI was calculated as follows: **PGI = 100−GP**.

cationic interaction with the residue Lys352 plays an important role in many approved anticancer drugs. For instance, sorafenib, a drug approved to treat liver cancer, interacts with a positively charged lysine residue of human p38 MAP kinase, and lapatinib, a drug approved to treat breast cancer, interacts with a positively charged lysine residue of ErbB4

https://doi.org/10.1021/acsomega.3c01462
ACS Omega 2023, 8, 26837−26849

Table 6. Molecular Docking Results of Oxadiazole Analogues against Tubulin (PDB ID: 5LYJ)

s. no.	compound	docking score (Kcal/mol)	Glide emodel	main electrostatic interactions
1	**6a**	−8.333	−59.246	H-bond (Asn258; 2.59 Å)
2	**6b**	−8.015	−59.983	H-bond (Asp251; 2.76 Å)
3	**6c**	−7.803	−60.283	
4	**6d**	−8.073	−63.376	
5	**6e**	−7.795	−61.691	
6	**6f**	−8.557	−62.839	H-bond (Asn258; 2.66 Å)
7	**6g**	−8.558	−69.876	H-bond (Asn258; 2.61 Å); π-cationic (Lys352; 6.59 Å)
8	**6h**	−8.144	−56.749	π-cationic (Lys352; 6.59 Å)
9	**6i**	−8.839	−59.598	H-bond (Asn258; 2.30 Å)
10	**6j**	−8.519	−63.352	
11	combretastatin A4	−8.758	−67.558	

kinase through π−cationic interaction.[69,70] According to previously published research, the lead compound showed the most effective inhibition of tubulin polymerization with an IC_{50} value of 1.15 ± 0.06 M. It also significantly interacted with the Lys352 residue via a π−cation interaction in addition to H-bonds with other residues within the colchicine binding site of tubulin.[71] The ligand **6h** displayed a π−cationic interaction with the residue Lys352 and showed the most promising anticancer activity in the current investigation.

3.5. Molecular Dynamics Studies. The most active molecule **6h** was chosen as a model for sequence studies.

3.4.1. MD Simulation. The stability of compound **6h** and the reference drug combretastatin A4 inside the active pocket of tubulin as well as the dynamics of ligand−protein complexes was examined using a 100 ns MD simulation study. The parameters root-mean-square deviation (RMSD), root-mean-square fluctuation (RMSF), radius of gyration (R_g), solvent-accessible surface area (SASA), and H-bond analysis were used to evaluate the docked complexes.

3.4.2. Root-Mean-Square Deviation (RMSD). The amount of time required by the simulated system to reach structural equilibrium is determined using the RMSD method. It is a crucial parameter for determining how a protein's molecular conformation shifts or fluctuates in response to ligand binding. A 100 ns MD simulation was used to calculate the ligand and protein backbone RMSD in order to estimate the equilibrium time for simulated coupled protein−ligand complexes. All systems were in equilibrium after about ∼8 ns, and the protein backbone deviated significantly during the initial 10 ns of the simulation, from 4.34 to 7.26 nm, as would be expected given the abrupt change in the protein's environment. Afterward, the ligand−protein complexes were stabilized and demonstrated a steady-state dynamic behavior. The RMSD fluctuation pattern of the ligand **6h** complex was similar to that of the reference complex, combretastatin A4. The computed RMSD values are displayed in Figure 6A,B.

3.4.3. RMSFs. The RMSF parameter measures a residue's influence on a complex structure's fluctuation. The protein backbone showed very little variation in the RMSF values for the ligand **6h** and combretastatin A4 complexes (Figure S2A). When compared to the reference complex, the majority of the interrupted residues were discovered in loop regions far from the ligand binding pockets.

3.4.4. R_g. R_g was calculated by computing the protein's molecular volume and density. The calculated R_g of the ligand **6h** complex exhibited normal behavior in comparison to the combretastatin A4 complex, confirming a stable binding mode inside the binding pocket and agreeing with the RMSD outcomes (Figure S2B). It is interesting to note that the average R_g value for the ligand **6h** complex was comparable to that for the combretastatin A4 complex, demonstrating a steadying and stabilizing secondary structure in the protein, revealing a stable conformation within the binding pocket.

3.4.5. SASA. SASA is a significant parameter that denotes the steadiness of the ligand within the active site of the

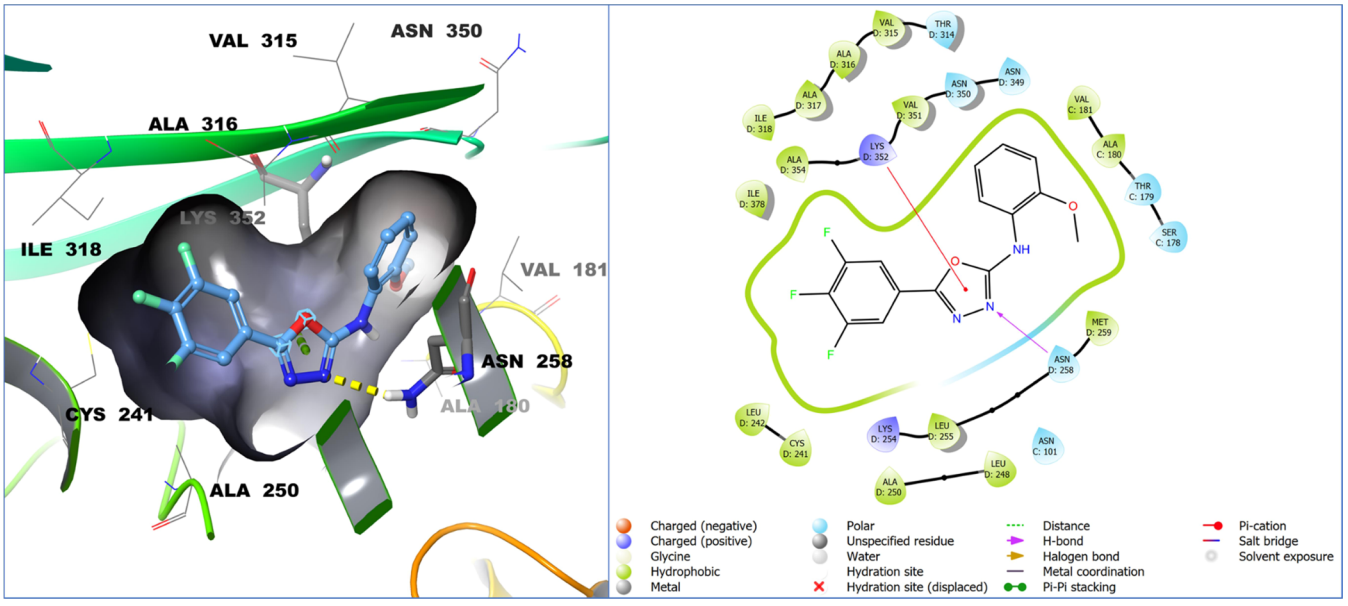

Figure 4. 3D and 2D Interactions of ligand **6g** within the binding site of combretastatin A4 of tubulin.

https://doi.org/10.1021/acsomega.3c01462
ACS Omega 2023, 8, 26837−26849

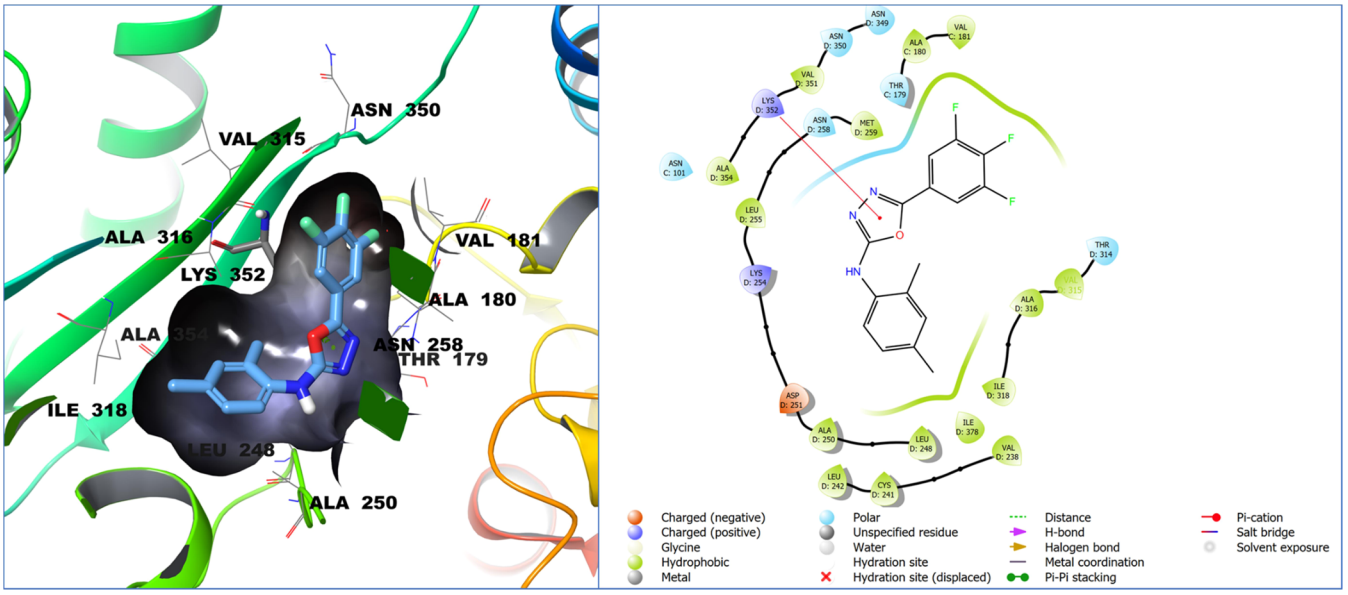

Figure 5. 3D and 2D Interactions of the ligand **6h** within the binding site of combretastatin A4 of tubulin.

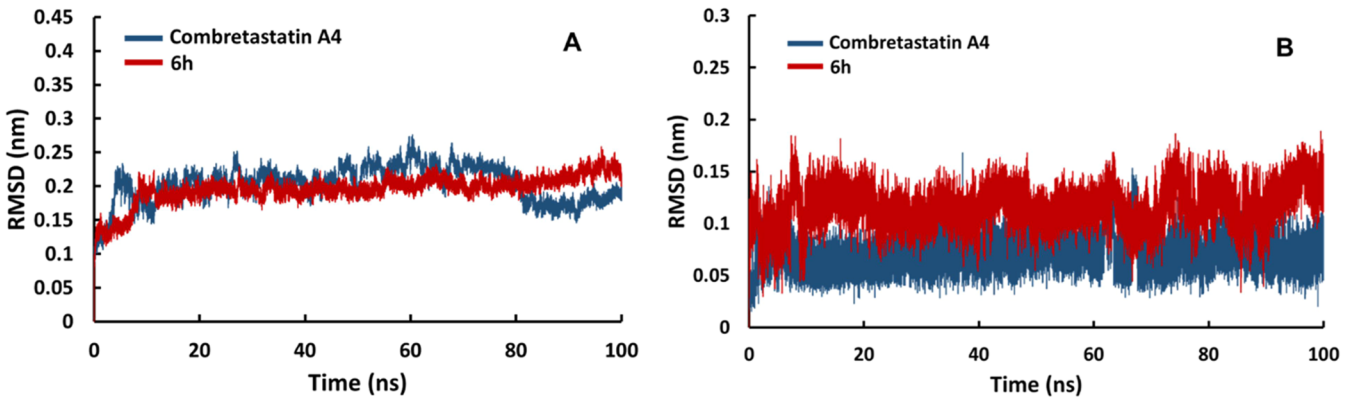

Figure 6. Comparison and detailed representation of (A) backbone RMSD and (B) ligand RMSD.

receptor. Greater ligand attraction within the active site is made possible by the large surface area. Subsequent to 100 ns of simulation, the ligand complexes' SASA values were calculated to see if the active site has adequate area for ligand binding. The reference substance (combretastatin A4) and ligand **6h** both kept their total surface areas stable and similar over the course of the simulation's 100 ns (Figure S2C). Therefore, they were identified as potential protein ligands.

3.4.6. Hydrogen-Bond Analysis. H-bonding plays an important role in keeping small molecules inside the active pocket of the protein in a stable conformation.[72] In comparison to combretastatin A4, the ligand **6h** had an average of more H-bonds during the 100 ns simulation. Figure S2D shows the H-bonds for both systems for a period of 100 ns during the simulation.

4. CONCLUSIONS

A series of 10 new oxadiazoles (**6a**−**j**) were prepared, each containing the basic pharmacophore two aryl rings linked with the oxadiazole moiety, as seen in the anticancer agents IMC-038525, IMC-094332, and FATB. The infrared (IR), nuclear magnetic resonance (NMR), and mass spectral data were used to characterize all of the oxadiazole analogues, and then, their ADME and toxicity studies were performed. Each oxadiazole analogue followed Lipinski's rule of five and had a low toxicity profile (class IV compounds). The antiproliferative action of the oxadiazole analogues (**6a**−**j**) was studied against 58 or 59 NCI cell lines of cancer. The compounds **6d** and **6i** demonstrated the most promising anticancer activity against the breast cancer cell line MCF7 with PGIs of 81.94 and 85.39, respectively. The most potent compound **6h** demonstrated good anticancer activity against three cancer cell lines, SNB-19, OVCAR-8, and NCI-H40 with PGIs of 86.61, 85.26, and 75.99, respectively; however, there was moderate anticancer activity against eight cancer cell lines, HOP-92, SNB-75, ACHN, NCI/ADR-RES, 786-O, A549/ATCC, HCT-116, and MDA-MB-231, with PGIs of 67.55, 65.46, 59.09, 59.02, 57.88, 56.88, 56.53, and 56.4, respectively, and less anticancer activity against 21 cancer cell lines, U251, NCI-H226, HS 578T, OVCAR-4, SF-268, NCI-H322M, RXF 393, CAKI-1, SK-OV-3, UO-31, SF-539, NCI-H522, SN12C, NCI-H23, PC-3, HOP-92, DU-145, IGROV1, EKXVA, OVCAR-3, and SK-MEL-28 with PGIs of 49.65, 49.55, 48.22, 48.19, 48.16, 45.92, 44.96, 41.91, 41.46, 40.82, 35.31, 30.22, 28.43, 25.81, 23.09, 22.86, 22.13, 21.44, 21.2, 21.18, and 21.05, respectively. Both the compound **6h**'s anticancer activity against the CNS cancer cell lines SNB-19, SNB-75, and SF-295 and its prediction that it will cross the blood−brain barrier are in perfect agreement.

https://doi.org/10.1021/acsomega.3c01462
ACS Omega 2023, 8, 26837−26849

The oxadiazole analogues **6h** also registered better anticancer activity than the reference drug Imatinib against CNS, non-small-cell lung, ovarian, renal, breast, prostate, and melanoma cancers. Furthermore, docking scores for the ligands, which ranged from −7.803 to −8.839 kcal/mol, showed that they efficiently bound to the tubulin active site (combretastatin A4 binding site). The docking studies revealed two types of interactions: H-bond and π−cationic. The ligand **6h** (docking score = −8.144 kcal/mol) interacted π-cationically with the residue Lys352 (with the oxadiazole ring) and had promising anticancer activity. The compounds **6d**, **6f**, and **6i** were found to have promising anticancer activity and had docking scores of −8.073, −8.557, and −8.839 kcal/mol, respectively, in the molecular docking studies. The compounds **6f** and **6i** have similar types of interactions in the molecular docking and had anticancer activity with mean GPs of 93 and 89.3 percent, respectively. The MD simulation studies in complex with the tubulin-combretastatin A4 protein and the ligand **6h** were performed to examine the dynamic stability and conformational behavior. The reference complex, combretastatin A4, and the ligand **6h** complex both had similar RMSD fluctuation patterns, and the RMSF values had a very little variation along the protein backbone. Comparing the calculated R_g of the ligand **6h** complex to the combretastatin A4 complex revealed a normal behavior, indicating a stable binding mode inside the binding pocket and correlating with the RMSD results. Throughout the simulation's 100 ns, the reference substance (combretastatin A4) and the ligand **6h** both maintained similar and stable total surface areas. In comparison to combretastatin A4, ligand **6h** had an average of more H-bonds during the 100 ns of simulation. The current study on the anticancer activity of 1,3,4-oxadiazoles and their in silico studies may add therapeutic value to oxadiazole because some of the compounds demonstrated promising antiproliferative activity against a few cancer cell lines. Additionally, the reported oxadiazoles can be modified further to increase their anticancer potentials.

■ ASSOCIATED CONTENT

Supporting Information

The Supporting Information is available free of charge at https://pubs.acs.org/doi/10.1021/acsomega.3c01462.

Synthetic procedure of intermediate compounds **3a−j**, **4a−j**, and **5a−j**; protocol for in vitro anticancer screening and molecular dynamic studies (Figure S1); 3D interaction of ligands **6a**, **6f**, and **6i** within the binding site of combretastatin A4 of tubulin (PDB ID: 5LYJ) (Figure S2); comparison and detailed representation of ligand **6h** and combretastatin A4 RMSF values, R_g trajectory, solvent-accessible surface area (SASA), and hydrogen-bond interactions (Figures S3−S12); anticancer data of all of the title compounds (**6a−j**) at 10 μM (Figures S13−S16); ^{1}H NMR of intermediate compounds **5a**, **5e**, **5h**, and **5i** (Figures S17−S54); ^{1}H NMR, ^{13}C NMR, mass, and IR spectra of all of the title compounds (**6a−j**) (Table S1); and anticancer activity of the oxadiazole analogues (**6a−j**) in terms of growth percent at 10 μM (PDF)

■ AUTHOR INFORMATION

Corresponding Authors

Vandana Sharma − *Department of Pharmaceutical Chemistry, Arya College of Pharmacy, Jaipur, Rajasthan 302 001, India*; Email: vanu4amit@gmail.com

Mohamed Jawed Ahsan − *Department of Pharmaceutical Chemistry, Maharishi Arvind College of Pharmacy, Jaipur, Rajasthan 302 039, India*; orcid.org/0000-0002-6919-5489; Email: jawedpharma@gmail.com

Authors

Mohit Agarwal − *Department of Pharmaceutical Chemistry, Arya College of Pharmacy, Jaipur, Rajasthan 302 001, India; Department of Pharmaceutical Chemistry, Nims Institute of Pharmacy, Nims University, Jaipur, Rajasthan 303 121, India*

Obaid Afzal − *Department of Pharmaceutical Chemistry, College of Pharmacy, Prince Sattam Bin Abdulaziz University, Al-Kharj 11942, Saudi Arabia*; orcid.org/0000-0002-4188-5592

Salahuddin − *Department of Pharmaceutical Chemistry, Noida Institute of Engineering and Technology (Pharmacy Institute), Greater Noida 201 306, India*; orcid.org/0000-0002-1868-8865

Abdulmalik Saleh Alfawaz Altamimi − *Department of Pharmaceutical Chemistry, College of Pharmacy, Prince Sattam Bin Abdulaziz University, Al-Kharj 11942, Saudi Arabia*

Mubarak A. Alamri − *Department of Pharmaceutical Chemistry, College of Pharmacy, Prince Sattam Bin Abdulaziz University, Al-Kharj 11942, Saudi Arabia*

Manal A. Alossaimi − *Department of Pharmaceutical Chemistry, College of Pharmacy, Prince Sattam Bin Abdulaziz University, Al-Kharj 11942, Saudi Arabia*

Complete contact information is available at: https://pubs.acs.org/10.1021/acsomega.3c01462

Notes

The authors declare no competing financial interest.

■ ACKNOWLEDGMENTS

This study was supported via funding from Prince Sattam Bin Abdulaziz University project number (PSAU/2023/R/1444).

■ LIST OF ABBREVIATIONS

μM, micromole; Abs, absorption; ADME, absorption, distribution, metabolism, and excretion; BBB, blood−brain barrier; CNS, central nervous system; DCM, dichloromethane; DMSO, dimethyl sulfoxide; FATB, 2-(4-fluorophenyloamino)-5-(2,4-dihydroxyphenyl)-1,3,4-thiadiazole; GI, gastrointestinal; GP, growth percent; HBA, hydrogen-bond acceptor; HBD, hydrogen-bond donor; IR, infrared; LD, lethal dose; MD, molecular dynamic; MHz, megahertz; mmol, millimole; Mp, melting point; M_W, molecular weight; NCI, National Cancer Institute; NMR, nuclear magnetic resonance; NROTB, number of rotatable bond; NSC, National Service Center; PDB, Protein Data Bank; PGI, percent growth inhibition; ppm, parts per million; R_g, radius of gyration; RMSD, root-mean-square deviation; RMSF, root-mean-square fluctuation; SAR, structure−activity relationship; SASA, solvent-accessible surface area; TLC, thin-layer chromatography; TPSA, total polar surface area; UV, ultraviolet

https://doi.org/10.1021/acsomega.3c01462
ACS Omega 2023, 8, 26837−26849

REFERENCES

(1) Sung, H.; Ferley, J.; Siegel, R. L.; Laversanne, M.; Soerjomartaram, I.; Jemal, A.; Bray, F. Global cancer statistics 2020: GLOBOCAN estimates of incidence and mortality worldwide for 36 cancers in 185 countries. *Ca-Cancer J. Clin.* **2021**, *71*, 209−249.

(2) Siegel, R. L.; Miller, K. D.; Fuchs, H. E.; Jemal, A. Cancer statistics, 2022. *Ca-Cancer J. Clin.* **2022**, *72*, 7−33.

(3) Sathishkumar, K.; Chaturvedi, M.; Das, P.; Stephen, S.; Mathur, P. Cancer incidence estimates for 2022 & projection for 2025: Result from National Cancer Registry Programme, India. *Indian J. Med. Res.* **2022**, *156*, 598−607.

(4) Debela, D. T.; Muzazu, S. G. Y.; Heraro, K. D.; Ndalama, M. T.; Mesele, B. W.; Haile, D. C.; Kitui, S. K.; Manyazewal, T. New approaches and procedures for cancer treatment: Current perspectives. *SAGE Open Med.* **2021**, *9*, No. 205031212110343.

(5) Baskar, R.; Yap, S. P.; Chua, K. L. M.; Itahana, K. The diverse and complex roles of radiation on cancer treatment: therapeutic target and genome maintenance. *Am J. Cancer Res.* **2012**, *2*, 372−382.

(6) Schirrmacher, V. From chemotherapy to biological therapy: A review of novel concepts to reduce the side effects of systemic cancer treatment (Review). *Int. J. Oncol.* **2018**, *54*, 407−419.

(7) Kumar, V.; Mudgal, M. M.; Rani, N.; Jha, A.; Jaggi, M.; Singh, A. T.; Sanna, V. K.; Singh, P.; Sharma, P. K.; Irchhaiya, R.; Burman, A.C.J. *J. Enzyme Inhib. Med. Chem.* **2009**, *24*, 763−770.

(8) Arthur, D. E.; Uzairu, A.; Mamza, P.; Abechi, S. Quantitative structure−activity relationship study on potent anticancer compounds against MOLT-4 and P388 leukemia cell lines. *J. Adv. Res.* **2016**, *7*, 823−837.

(9) Vaidya, A.; Jain, S.; Jain, P.; Jain, P.; Tiwari, N.; Jain, R.; Jain, R.; Jain, A.; Agrawal, R. K. Synthesis and biological activities of oxadiazole derivatives: a review. *Mini-Rev. Med. Chem.* **2016**, *16*, 825−845.

(10) Namee, N. M.; Driscoll, L. O. Extracellular vesicles and anti-cancer drug resistance. *Biochim. Biophys. Acta, Rev. Cancer* **2018**, *1870*, 123−136.

(11) Szumilak, M.; Wiktorowska-Owczarek, A.; Stanczak, A. Hybrid Drugs-A Strategy for Overcoming Anticancer Drug Resistance? *Molecules* **2021**, *26*, No. 2601.

(12) Thanikachalam, P. V.; Maurya, R. K.; Garg, V.; Monga, V. An insight into the medicinal perspective of synthetic analogs of indole: A review. *Eur. J. Med. Chem.* **2019**, *180*, 562−612.

(13) Kakkar, S.; Narasimhan, B. A comprehensive review on biological activities of oxazole derivatives. *BMC Chem.* **2019**, *13*, No. 16.

(14) Mandewale, M. C.; Patil, U. C.; Shedge, S. V.; Dappadwad, U. R.; Yamgar, R. S. A review on quinoline hydrazone derivatives as a new class of potent antitubercular and anticancer agents. *Beni-Suef Univ. J. Basic Appl. Sci.* **2017**, *6*, 354−361.

(15) Xu, Z.; Zhao, S. J.; Liu, Y. 1,2,3-Triazole-containing hybrids as potential anticancer agents: Current developments, action mechanisms and structure-activity relationships. *Eur. J. Med. Chem.* **2109**, *183*, No. 111700.

(16) (a) Nayak, S.; Gaonkar, S. L. A Review on Recent Synthetic Strategies and Pharmacological Importance of 1,3-Thiazole Derivatives. *Mini-Rev. Med. Chem.* **2019**, *19*, 215−238. (b) Nayak, S.; Gaonkar, S. L.; Musad, E. A.; Al-Dawsar, A. M. 1,3,4-Oxadiazole-containing hybrids as potential anticancer agents: Recent developments, mechanism of action and structure-activity relationships. *J. Saudi Chem. Soc.* **2021**, *25*, No. 101284.

(17) Ahsan, M. J. 1,3,4-Oxadiazole containing compounds as therapeutic targets for cancer therapy. *Mini-Rev. Med. Chem.* **2022**, *22*, 144−197.

(18) Boström, J.; Hogner, A.; Llinàs, A.; Wellner, E.; Plowright, A. T. Oxadiazoles in medicinal chemistry. *J. Med. Chem.* **2012**, *55*, 1817−1830.

(19) Zhang, K.; Wang, P.; Xuan, L. N.; Fu, X. Y.; Jing, F.; Li, S.; Liu, Y. M.; Chen, B. Q. Synthesis and antitumor activities of novel hybrid molecules containing 1,3,4-oxadiazole and 1,3,4-thiadiazole bearing Schiff base moiety. *Bioorg. Med. Chem. Lett.* **2014**, *24*, 5154−5156.

(20) Agarwal, M.; Singh, V.; Sharma, S. K.; Sharma, P.; Ansari, M. Y.; Jadav, S. S.; Yasmin, S.; Sreenivasulu, R.; Hassan, M. Z.; Saini, V.; Ahsan, M. J. Design and synthesis of new 2,5-disubstituted-1,3,4-oxadiazole analogues as anticancer agents. *Med. Chem. Res.* **2016**, *25*, 2289−2303.

(21) Glomb, T.; Szymankiewicz, K.; Świątek, P. Anti-Cancer Activity of Derivatives of 1,3,4-Oxadiazole. *Molecules* **2018**, *23*, No. 3361.

(22) Paruch, K.; Popiołek, Ł.; Wujec, M. Antimicrobial and antiprotozoal activity of 3-acetyl-2,5-disubstituted-1,3,4-oxadiazolines: a review. *Med. Chem. Res.* **2020**, *29*, 1−16.

(23) De, S. S.; Khambete, M. P.; Degani, M. S. Oxadiazole scaffolds in anti-tuberculosis drug discovery. *Bioorg. Med. Chem. Lett.* **2019**, *29*, 1999−2007.

(24) Sondhi, S. M.; Kumar, S.; Kumar, N.; Roy, P. Synthesis anti-inflammatory and anticancer activity evaluation of some pyrazole and oxadiazole derivatives. *Med. Chem. Res.* **2012**, *21*, 3043−3052.

(25) Bhutani, R.; Pathak, D. P.; Kapoor, G.; Husain, A.; Iqbal, M. A. Novel hybrids of benzothiazole-1,3,4-oxadiazole-4-thiazolidinone: Synthesis, in silico ADME study, molecular docking and in vivo anti-diabetic assessment. *Bioorg. Chem.* **2019**, *83*, 6−19.

(26) Cui, Z. N.; Shi, Y. X.; Zhang, L.; Ling, Y.; Li, B. J.; Nishida, Y.; Yang, X. L. Synthesis and Fungicidal Activity of Novel 2,5-Disubstituted-1,3,4-oxadiazole Derivatives. *J. Agric. Food Chem.* **2012**, *60*, 11649−11656.

(27) Mihailović, N.; Markovic, V.; Matic, I. Z.; Stanisavljevic, N. S.; Jovanovic, Z. S.; Trifunovic, S.; Joksovic, L. Synthesis and Antioxidant Activity of 1,3,4-Oxadiazoles and Their Diacylhydrazine Precursors Derived from Phenolic Acids. *RSC Adv.* **2017**, *7*, 8550−8560.

(28) Tabatabai, S. A.; Lashkari, S. B.; Zarrindast, M. R.; Golibeikian, M.; Shafiee, A. Design, Synthesis and Anticonvulsant Activity of 2-(2-Phenoxy)phenyl-1,3,4-oxadiazole Derivatives. *Iranian J. Pharm. Sci.* **2013**, *12*, 105−111.

(29) Attaby, F. A.; Fattah, A. M. A.; Shaif, L. M.; Elsayed, M. M. Anti-Alzheimer and anti-Cox-2 Activities of the Newly Synthesized 2,3-Bipyridine Derivatives (II). *Phosphorus, Sulfur Silicon Relat. Elem.* **2010**, *185*, 668−679.

(30) Malhotra, V.; Pathak, S. R.; Nath, R.; Mukherjee, D.; Shanker, K. Substituted Imidazole Derivatives as Novel Cardiovascular Agents. *Bioorg. Med. Chem. Lett.* **2011**, *21*, 936−939.

(31) El-Sayed, W. A.; El-Essawy, F. A.; Ali, O. M.; Nasr, B. S.; Abdalla, M. M.; Abdel-Rahman, A. A. H. Synthesis and Antiviral Evaluation of New 2,5-Disubstituted 1,3,4-Oxadiazole Derivatives and Their Acyclic Nucleoside Analogues. *Monatsh. Chem.- Chem. Mon.* **2010**, *141*, 1021−1028.

(32) James, N. D.; Growcott, J. W. Zibotentan. *Drugs Future* **2009**, *34*, 624−633.

(33) Cocohoba, J.; Dong, B. J. Raltegravir: The First HIV Integrase Inhibitor. *Clin. Ther.* **2008**, *30*, 1747−1765.

(34) Schlecker, R.; Thieme, P. C. The synthesis of antihypertensive 3-(1,3,4-oxadiazol-2-yl)phenoxypropanolahines. *Tetrahedron* **1988**, *44*, 3289−3294.

(35) Ogata, M.; Atobe, H.; Kushida, H.; Yamamoto, K. In Vitro Sensitivity of Mycoplasmas Isolated From Various Animals and Sewage to Antibiotics and Nitrofurans. *J. Antibiot.* **1971**, *24*, 443−451.

(36) Li, Q.; Sham, H. L. Discovery and development of antimitotic agents that inhibit tubulin polymerisation for the treatment of cancer. *Expert Opin. Ther. Pat.* **2002**, *12*, 1663−1702.

(37) Lin, C. M.; Ho, H. H.; Pettit, G. R.; Hamel, E. Antimitotic natural products combretastatin A-4 and combretastatin A-2: studies on the mechanism of their inhibition of the binding of colchicine to tubulin. *Biochemistry* **1989**, *28*, 6984−6991.

(38) Mitchison, T. J.; Salmon, E. Mitosis: a history of division. *Nat. Cell Biol.* **2001**, *3*, E17−E21.

(39) Sayeed, I. B.; Nayak, V. L.; Shareef, M. A.; Chouhan, N. K.; Kamal, A. Design, synthesis and biological evaluation of imidazopyridine-propenone conjugates as potent tubulin inhibitors. *MedChemComm* **2017**, *8*, 1000−1006.

(40) Kamal, A.; Shaik, A. B.; Polepalli, S.; Reddy, V. S.; Kumar, G. B.; Gupta, S.; Krishna, K.V.S.R.; Nagabhushana, A.; Mishra, R. K.;

https://doi.org/10.1021/acsomega.3c01462
ACS Omega 2023, 8, 26837−26849

Jain, N. Pyrazole−oxadiazole conjugates: synthesis, antiproliferative activity and inhibition of tubulin polymerization. *Org. Biomol. Chem.* **2014**, *12*, 7993−8007.
(41) Nayak, S.; Gaonkar, S. L.; Musad, E. A.; Dawsar, A. M. A. L. 1,3,4-Oxadiazole-containing hybrids as potential anticancer agents: Recent developments, mechanism of action and structure-activity relationships. *J. Saudi Chem. Soc.* **2021**, *25*, No. 101284.
(42) Abdel-Aziz, M.; Metwally, K. A.; Gamal-Eldeen, A. M.; Aly, O. M. 1,3,4-oxadiazole-2-thione Derivatives; Novel Approach for Anticancer and Tubulin Polymerization Inhibitory Activities. *Anti-Cancer Agents Med. Chem.* **2015**, *16*, 269−277.
(43) Bohm, H. J.; Flohr, A.; Stahl, M. Scaffold hoping. *Drug Discovery Today: Technol.* **2004**, *1*, 217−224.
(44) Tuma, C. M.; Malikzay, A.; Ouyang, X.; Surguladze, D.; Fleming, J.; Mitelman, S.; Camara, M.; Finnerty, B.; Doody, J.; Chekler, E. L. P.; Kussie, P.; Tonra, J. R. Antitumor activity of IMC-038525, a novel oral tubulin polymerization inhibitor. *Transl. Oncol.* **2010**, *3*, 318−325.
(45) Juszczak, M.; Matysiak, J.; Szeliga, M.; Pozarowski, P.; Niewiadomy, A.; Albrecht, J.; Rzeski, W. 2-Amino-1,3,4-thiadiazole derivative (FABT) inhibits extracellular signal-regulated kinase pathway and induces cell cycle arrest in human non-small lung carcinoma cells. *Bioorg. Med. Chem. Lett.* **2012**, *22*, 5466−5469.
(46) Ahsan, M. J.; Sharma, J.; Singh, M.; Jadav, S. S.; Yasmin, S. Synthesis and anticancer activity of *N*-aryl-5-substituted-1,3,4-oxadiazol-2-amine analogues. *BioMed Res. Int.* **2014**, *2014*, 1−9.
(47) Salahuddin, M.; Shaharyar, A.; Majumdar, A.; Ahsan, M. J. Synthesis, characterization and anticancer evaluation of 2-(naphthalen-1-ylmethyl/naphthalen-2-yloxymethyl)-1-[5-(substituted phenyl)-[1,3,4]oxadiazol-2-ylmethyl]-1H-benzimidazole. *Arabian J. Chem.* **2014**, *7*, 418−424.
(48) Swiss ADME http://www.swissadme.ch/ (retrieved on January 21, 2023).
(49) ProTox II https://tox-new.charite.de/protox_II/index.php?site=compound_input (retrieved on January 21, 2023).
(50) Boyd, M. R.; Paull, K. D. Some practical considerations and applications of the National Cancer Institute *in vitro* anticancer drug discovery screen. *Drug Dev. Res.* **1995**, *34*, 91−109.
(51) Monks, A.; Scudiero, D.; Skehan, P.; Shoemaker, R.; Paull, K.; Vistica, D.; Hose, C.; Langley, J.; Cronise, P.; Vaigro-Wolff, A.; Gray-Goodrich, M.; Campbell, H.; Mayo, J.; Boyd, M. Feasibility of a highflux anticancer drug screening using a diverse panel of cultured human tumor cell lines. *J. Nat. Cancer Inst.* **1991**, *83*, 757−766.
(52) Shoemaker, R. H. The NCI60 human tumour cell line anticancer drug screen. *Nat. Rev. Cancer* **2006**, *6*, 813−823.
(53) (a) NCI-60 Screening Methodology. Retrieved from: https://dtp.cancer.gov/discovery_development/nci-60/methodology.html. (Retrieved on April 05, 2023). (b) NCI database compound ID NSC 759854 (Imatinib). Retrieved from: https://dtp.cancer.gov. (Retrieved on November 13, 2020).
(54) X-ray crystallographic structure of tubulin-combrestatin A4 complex. https://www.rcsb.org/structure/5lyj. (Retrieved on January 12, 2023).
(55) Gaspari, R.; Prota, A. E.; Bargsten, K.; Cavalli, A.; Steinmetz, M. O. Structural Basis of cis - and trans -Combretastatin Binding to Tubulin. *Chem* **2017**, *2*, 102−113.
(56) Van Der Spoel, D.; Lindahl, E.; Hess, B.; Groenhof, G.; Mark, A. E.; Berendsen, H. J. GROMACS: fast, flexible, and free. *J. Comput. Chem.* **2005**, *26*, 1701−1718.
(57) Zoete, V.; Cuendet, M. A.; Grosdidier, A.; Michielin, O. SwissParam: a fast force field generation tool for small organic molecules. *J. Comput. Chem.* **2011**, *32*, 2359−2368.
(58) Yogeeswari, P.; Sriram, D.; Thirumurugan, R.; Saxena, A.; Stables, J.; Vaigunda, J.; Raghuvendran; Suddan, K.; Pavana, R. K. Discovery of N-(2,6-Dimethyphenyl)-substituted semicarbazones as Anticonvulsants: Hybrid Pharmacophore-Based Design. *J. Med. Chem.* **2005**, *48*, 6202−6211.
(59) Ahsan, M. J.; Hassan, M. Z.; Jadav, S. S.; Geesi, M. H.; Bakht, M. A.; Riadi, Y.; Salahuddin; Akhtar, M. S.; Nasr, M.; Akhter, M. H. Synthesis and biological potentials of 5-aryl-N-[4-(trifluoromethyl)-phenyl]-1,3,4-oxadiazol-2-amines. *Lett. Org. Chem.* **2020**, *17*, 133−140.
(60) Ahsan, M. J.; Khalilullah, H.; Yasmin, S.; Jadav, S. S.; Stables, J. P.; Govindasamy, J. Synthesis and anticonvulsant evaluation of 2-(substituted benzylidene/ethylidene)-N-(substituted phenyl)-hydrazine-carboxamide analogues. *Med. Chem. Res.* **2013**, *22*, 2746−2754.
(61) Lee, H. G.; Kim, M. J.; Park, S. E.; Kim, J. J.; Kim, B. J.; Lee, S. G.; Yoon, Y. J. Phenyl 4,5-Dichloro-6-Oxopyridazine-1(6H)-Carboxylate as Carbonyl Source: Facile and Selective Synthesis of Carbamates and Ureas under Mild Conditions. *Synlett* **2009**, *17*, 2809−2814.
(62) Yogeeswari, P.; Ragavendran, J. V.; Thirumurugan, R.; Induja, S.; Sriram, D.; Stables, J. P. Synthesis and Structure-Activity Relationship on Anticonvulsant Aryl Semicarbazones. *Med. Chem.* **2006**, *2*, 55−62.
(63) Pandeya, S. N.; Yogeeswari, P.; Stable, J. P. Synthesis and anticonvulsant activity of 4-bromophenyl substituted aryl semicarbazones. *Eur. J. Med. Chem.* **2000**, *35*, 879−886.
(64) Amir, M.; Ahsan, M. J.; Ali, I. Synthesis of N^1-(3-chloro-4-flourophenyl)-N^4-substituted semicarbazones as novel anticonvulsant agents. *Indian J. Chem.* **2010**, *49B*, 1509−1514.
(65) Lipinski, C. A.; Lombardo, L.; Dominy, B. W.; Feeney, P. J. Experimental and computational approaches to estimate solubility and permeability in drug discovery and development settings. *Adv. Drug Delivery Rev.* **2001**, *46*, 3−26.
(66) Ertl, P.; Rohde, B.; Selzer, P. Fast calculation of molecular polar surface area as a sum of fragment-based contributions and its application to the prediction of drug transport properties. *J. Med. Chem.* **2000**, *43*, 3714−3717.
(67) Corona, P.; Carta, A.; Loriga, M.; Vitale, G.; Paglietti, G. Synthesis and in-vitro antitumor activity of new quinoxaline derivatives. *Eur. J. Med. Chem.* **2009**, *44*, 1579−1591.
(68) Jordan, A.; Hadfield, J. A.; Lawrence, N. J.; McGown, A. T. Tubulin as a target for anticancer drugs: Agents which interact with the mitotic spindle. *Med. Res. Rev.* **1998**, *18*, 259−296.
(69) Simard, J. R.; Getlik, M.; Grutter, C.; Pawar, V.; Wulfert, S.; Rabiller, M.; Rauh, D. Development of a fluorescent-tagged kinase assay system for the detection and characterization of allosteric kinase inhibitors. *J. Am. Chem. Soc.* **2009**, *131*, 13286−13296.
(70) Qiu, C.; Tarrant, M. K.; Choi, S. H.; Sathyamurthy, A.; Bose, R.; Banjade, S.; Pal, A.; Bornmann, W. G.; Lemmon, M. A.; Cole, P. A.; Leahy, D. J. Mechanism of activation and inhibition of the HER4/ErbB4 kinase. *Structure* **2008**, *16*, 460−467.
(71) Alam, M. J.; Alam, O.; Perwez, A.; Rizvi, M. A.; Naim, M. J.; Naidu, V. G. M.; Imran, M.; Ghoneim, M. M.; Alshehri, S.; Shakeel, F. Design, Synthesis, Molecular Docking, and Biological Evaluation of Pyrazole Hybrid Chalcone Conjugates as Potential Anticancer Agents and Tubulin Polymerization Inhibitors. *Pharmaceuticals* **2022**, *15*, No. 280.
(72) Kamaraj, B.; Bogaerts, A. Structure and Function of p53-DNA Complexes with Inactivation and Rescue Mutations: A Molecular Dynamics Simulation Study. *PLoS One* **2015**, *10*, No. e0134638.

https://doi.org/10.1021/acsomega.3c01462
ACS Omega 2023, 8, 26837−26849